GEMIR: Graph-Based Joint Modeling of Electromigration and IR Drop for Power Grid

Feng Guo*
Beijing University of Posts and Telecommunications
China

Yueyue Xi*
Beijing University of Posts and Telecommunications
China

Jingyu Jia
Beijing University of Posts and Telecommunications
China

Jiawei Liu
The Chinese University of Hong Kong
China

Tianshu Hou
The Chinese University of Hong Kong
China

Yuyang Ye
The Chinese University of Hong Kong
China

Jianwang Zhai†
Beijing University of Posts and Telecommunications
China

Kang Zhao
Beijing University of Posts and Telecommunications
China

Chuan Shi
Beijing University of Posts and Telecommunications
China

Abstract

The combined effects of electromigration (EM) and IR drop critically affect the reliability and power integrity of power grids (PGs). Existing numerical methods are computationally prohibitive for large-scale designs, while most machine learning (ML) approaches analyze EM and IR drop in isolation, overlooking their shared physical structure and correlations in practical flows. To address this limitation, we propose GEMIR, a graph-based multi-task learning framework for the joint prediction of node-level static IR drop and edge-level EM-induced stress. GEMIR employs a cross-layer node-edge attention mechanism to effectively capture the mutual dependence between these two physical fields and integrates a physics-informed neural network (PINN) to enhance physical consistency in the EM path. Furthermore, we establish a composite optimization objective by incorporating physics-informed constraints that embed Kirchhoff's current law (KCL) and Korhonen's PDE to enhance model interpretability. To manage the inherently coupled yet sometimes conflicting optimization dynamics resulting from these constraints, we then develop a Conflict-Gated (CG) multi-task optimization that adaptively fuses or decouples task gradients based on their alignment, thereby achieving mutual optimality. Extensive experiments demonstrate that GEMIR outperforms existing single-task and multi-task baselines in accuracy and generalization.

Keywords

Power Grid, IR Drop, Electromigration

ACM Reference Format:
Feng Guo, Yueyue Xi, Jingyu Jia, Jiawei Liu, Tianshu Hou, Yuyang Ye, Jianwang Zhai, Kang Zhao, and Chuan Shi. 2026. GEMIR: Graph-Based Joint Modeling of Electromigration and IR Drop for Power Grid . In *63rd ACM/IEEE Design Automation Conference (DAC '26), July 26–29, 2026, Long Beach, CA, USA*. ACM, New York, NY, USA, 7 pages. https://doi.org/10.1145/3770743.3803897

*These authors contributed equally.
†Corresponding author.

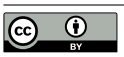

DAC '26, Long Beach, CA, USA

ACM ISBN 979-8-4007-2254-7/2026/07
https://doi.org/10.1145/3770743.3803897

1 Introduction

As semiconductor chips continue to scale down, electromigration-induced stress in interconnects and voltage drop (IR drop) across power grids (PGs) have become critical threats to the performance, reliability, and power integrity of chips [10, 17, 19, 24]. High local IR drop, for instance, raises metal temperature and resistivity, which in turn drives current crowding. This current crowding directly accelerates atomic flux divergence, a process intimately connected to EM. Conversely, EM-induced void spanning forces current into the more resistive liner, causing a resistance jump and consequent IR drop, as shown in Figure 1. This mutually influential relationship between EM and IR drop poses significant challenges for ensuring robust chip reliability and power integrity. Consequently, efficient and accurate EM-IR joint analysis becomes crucial.

Traditionally, EM and IR drop validations rely on numerical methods that solve large-scale linear systems and partial differential equations (PDEs). These methods, however, demand substantial computational resources and time cost, making them impractical for large-scale industrial designs, especially in the early design stages [22]. Recently, many machine learning (ML)-based methods have been proposed to accelerate the EM and IR drop analysis process. For IR drop, recent image-based [7, 9, 20, 23] and graph-based [8, 25] approaches model PG in different forms to provide IR drop prediction in various grains. Similarly, EM analysis methods like EM-GAN [13] and EMGraph [12] transform EM-induced stress analysis into an image generation task and node regression in graphs. Moreover, considering the above data-driven methods lack physical interpretability, the physics-informed neural networks (PINNs) that incorporate PDE constraints with high computational complexity are used for in EM analysis [11, 15]. However, all the above approaches oversimplify the problem by treating EM and IR drop separately, thereby neglecting their physical correlation.

These two tasks share the underlying physical structure (e.g., PG) and physical driving factors. Critically, existing methods analyze EM and IR drop in isolation, failing to capitalize on their strong physical correlation. This oversight is significant, as treating

This work is supported by the National Natural Science Foundation of China (No. 62404021, 62550138, 62192784, 62572064, 62472329), the Beijing Natural Science Foundation (No. 4244107), the State Key Lab of Processors, Institute of Computing Technology, CAS (No. CLQ202504), the Fundamental Research Funds for the BUPT (No. 2025AI4S20), and the Research Initiation Project for Introduced Talents of BUPT (No. 510224062).

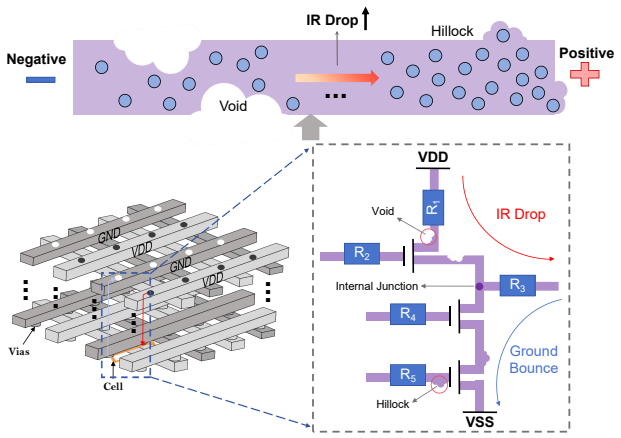

Figure 1: The illustration of the close and mutual relationship between IR drop and EM in PGs.

them independently neglects their physical interactions, which ultimately undermines prediction reliability and accuracy. For instance, the physical conditions that lead to EM-induced stress, such as high current crowding, are precisely the signals that can help predict elusive IR drop hotspots. Conversely, IR drop provides the essential voltage and current context required to accurately refine full-chip stress analysis. However, accurately modeling such a mutually influential relationship presents a significant challenge for current approaches. Thus, an approach that can model EM-IR simultaneously and perform accurate and efficient co-prediction is urgently required to meet the reliability demands of modern sign-off.

To address this, we propose GEMIR, a novel graph-based multi-task framework for co-predicting EM-induced stress and IR drop, which models their mutual correlation to improve prediction accuracy and reliability. We first represent the power grid (PG) as a directed graph with engineered node and edge features. To structurally correlate EM and IR drop and learn shared yet task-aware representations, we utilize a customized node and edge attention aggregator interconnected via a cross-task message-passing mechanism. This mechanism is further strengthened by integrating a PINN to enforce physical consistency. Finally, we augment the training objective with physics-informed constraints that embed KCL and Korhonen's PDE, thereby ensuring physical consistency and addressing the limitations of pure data-driven approaches. Specifically, to effectively manage the inherently coupled yet sometimes conflicting optimization dynamics resulting from these constraints, we propose a Conflict-Gated (CG) strategy. This strategy adaptively fuses or decouples task gradients based on their agreement, leading to superior prediction accuracy and enhanced generalization. Extensive experiments demonstrate that GEMIR achieves higher accuracy on both tasks than strong single-task and multi-task baselines, while preserving inference efficiency.

The key contributions are summarized as follows:

- We present GEMIR, a multi-task framework for the joint prediction of node-level IR drop and edge-level EM-induced stress. GEMIR leverages coupled yet task-aware representations learned via a cross-layer node-edge attention aggregator and integrated PINN, capturing the physical correlation between the two tasks.
- We introduce the CG strategy, a novel multi-task optimization that intelligently manages the joint learning process. By adaptively fusing synergistic gradients and decoupling conflicting updates, CG ensures a highly robust optimization, leading to superior prediction accuracy and enhanced generalization.
- Extensive experiments demonstrate that GEMIR achieves superior accuracy and generalization in co-predicting EM-induced stress and IR drop, outperforming strong single-task and multi-task baselines while maintaining high computational efficiency.

2 Preliminaries

2.1 Review of EM and IR Drop Analysis

EM refers to atomic migration in metal interconnects driven by current and temperature [2], potentially causing voids or hillocks that degrade circuit performance. Concurrently, IR drop emerges from current flowing through PG resistances [24], compromising power integrity and causing functional failures. These phenomena interact through a feedback loop: IR drop-induced Joule heating raises resistance and local current density, accelerating EM, while EM-induced voids further increase resistance, exacerbating IR drop. This cyclic interaction may ultimately lead to power delivery failure. Figure 1 illustrates this key interaction, showing how EM-induced voids and hillocks increase IR drop by altering current flow and resistance, and how IR drop in turn accelerates EM. Thus, accurate co-prediction that explicitly models the physical interaction between EM and IR drop is crucial for robust power integrity sign-off.

Traditional numerical methods typically employ Korhonen's PDE [14] to describe the evolution of stress $\sigma(\mathrm{x}, \mathrm{t})$. This foundational equation is extended to formulate the coupled EM-IR governing equation, formally expressed as:

$$\frac{\partial \sigma(\mathrm{x}, \mathrm{t})}{\partial t} = \frac{\partial}{\partial x}\left[\kappa\left(\frac{\partial \sigma(\mathrm{x}, \mathrm{t})}{\partial x} - \frac{eZ\rho j}{\Omega} - \frac{Q \cdot \eta I}{\Omega\left(T_0 + \eta I V\right)}\frac{\partial V}{\partial x}\right)\right], \quad (1)$$

where x denotes position along the metal interconnect, t represents time, $\kappa = \frac{D_a B \Omega}{k_B T}$ is the stress diffusion coefficient, $\frac{eZ\rho j}{\Omega}$ quantifies the electron wind force, Q describes the influence of temperature gradients on atomic migration, T_0 is the initial temperature, η is a coefficient related to Joule heating, V indicates the IR drop of nodes, and I is the current through the interconnect. This equation is derived as an extended form of the classical Korhonen's PDE by incorporating Joule heating effects [26], where the temperature is expressed in terms of I and V via a thermo-electric analogy defined by $T = T_0 + \eta I V$. From the perspective of derivation, this process is indeed much more computationally intensive than a simulation that only considers the effects of EM. More importantly, the mutual influence of EM and IR drop on each other fundamentally increases the difficulty of simultaneous and accurate modeling for analysis.

2.2 Problem Definition

This work aims to model the relationship between EM and IR drop, enabling simultaneous prediction of steady-state EM-induced stress and static IR drop for efficient PG analysis. The PG is regarded as a directed graph $\mathcal{G} = (\mathcal{V}, \mathcal{E})$, where $\mathcal{V}$ denotes nodes (junctions) and $\mathcal{E}$ denotes current-carrying wires (branches). Our goal is to design a graph-based multi-task algorithm f_θ that leverages inter-task correlations. Given node and edge features of $\mathcal{G}$, f_θ outputs node-level IR drop predictions $\hat{V}$ and edge-level EM-induced stress predictions $\hat{\sigma}$, aiming to align closely with ground truth.

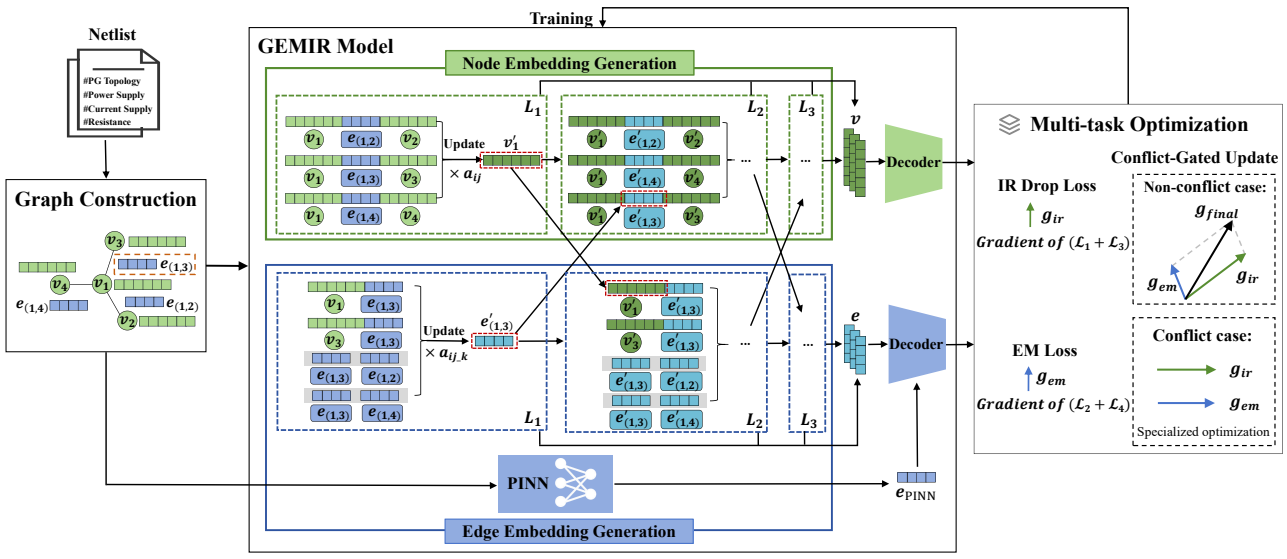

Figure 2: An Illustration of the GEMIR framework for IR drop and EM-induced stress co-prediction.

3 Methodologies

3.1 Overall Flow

To jointly and accurately model IR drop and EM as two correlated physical fields on the PG, we propose GEMIR, a graph-based framework designed explicitly for the co-prediction of node-level IR drop and edge-level EM-induced stress as illustrated in Figure 2. In our framework, PG is represented as a directed graph with separately extracted node and interconnect features. Then, we employ node and edge attention aggregators, interconnected via a cross-task message-passing mechanism. This design structurally builds shared yet task-aware representations and correlates the node-level IR drop with the edge-level EM-induced stress through the PG structure. In addition, we integrate a PINN architecture within the edge embedding generation to embed fundamental physical laws directly into the learning process, significantly improving model interpretability. During training, GEMIR optimizes a composite objective that combines data-driven losses for IR drop and EM with physics-informed losses derived from KCL and Korhonen's PDE. To handle the optimization of these related but not always perfectly aligned tasks, we introduce a Conflict-Gated multi-task optimization that intelligently manages the joint knowledge learning process. By adaptively fusing synergistic gradients and decoupling conflicting updates, the CG strategy ensures a robust optimization process that achieves both superior accuracy and strong generalization.

3.2 Graph Construction

To effectively and simultaneously represent IR drop and EM consistently on the PG structure, we first transform the PG into a directed graph representation, denoted as $\mathcal{G} = (\mathcal{V}, \mathcal{E})$. We extract critical node and edge features to represent knowledge from PG netlists, as shown in Table 1. In particular, we embed two distinct forms of positional knowledge into node features, as the model must understand both geometric (spatial) and electrical (physical) relations. To capture the node's absolute geometric coordinates (x, y) on the chip, where physically close nodes influence each other, we generate geometric positional encoding PE_{geo}. We use a sinusoidal encoding function to map these continuous coordinates into a high-dimensional vector. To capture a node's circuit position in the PG, we calculate the first three shortest path resistances R_{eff} to the nearest power supplier and encode it into electrical positional encoding as $\boldsymbol{PE_{elec}(v)} = \left[\boldsymbol{R_{eff}}\,(v, p_1)\,, \boldsymbol{R_{eff}}\,(v, p_2)\,, \boldsymbol{R_{eff}}\,(v, p_3)\right]$. The extraction and selection of these features are based on circuit knowledge and feature correlation comparison in graphs. The label values of $\mathcal{V}$ are IR drops, and $\mathcal{E}$ is labeled with stress sampled at five equidistant points (0%, 25%, 50%, 75%, 100%) along each interconnect segment.

Table 1: Extracted Node and Edge Features.

Type	Symbol	Description
Node	I_N	Node current calculated by KCL
	C_N	Network type (0: VDD, 1: GND)
	C_M	Metal layer of the node (e.g., 0: M0)
	PE_{geo}	Geometric positional encoding
	PE_{elec}	Electrical positional encoding
	D_r	Node degree (in-degree + out-degree)
	E_i	Eigenvector centrality
Edge	R	Wire resistance
	I_E	Current on the wire
	L	Wire length
	W	Wire width
	C_E	Edge direction (current direction)

3.3 Proposed Model

In this work, we present GEMIR, a novel multi-task model designed to co-predict EM-induced stress and IR drop by explicitly modeling their interdependence. The model takes the directed graph structure defined in Section 3.2 as input, incorporating both node and edge features. We design novel node and edge attention aggregators, equipped with a cross-task message-passing mechanism to capture the relationship between IR drop on nodes and stress on edges. To enhance physical consistency and interpretability, we

integrate a PINN. As shown in Figure 2, the PINN generates physics-constrained EM embeddings along the interconnects, concatenated with embeddings from the edge attention aggregator. Finally, to obtain predictions simultaneously, the output embeddings of nodes and edges are processed through MLP decoding steps.

Node Embedding Generation. Given the node representations $\left\{\boldsymbol{v}_i^l, \forall i \in N_v\right\}$ and edge representations $\left\{\boldsymbol{e}_{ij}^l, \forall (i,j) \in N_e\right\}$ generated by a linear transformer as input, the designed node attention aggregator (NAA) learns node and edge features jointly as:

$$\boldsymbol{v}_i^{l+1} = NAA\left(\left\{\boldsymbol{v}_i^l, \forall i \in N_v\right\}, \left\{\boldsymbol{e}_{ij}^l, \forall (i,j) \in N_e\right\}\right). \tag{2}$$

Here, the NAA embeds the relationship between EM and IR drop in output node representations $\left\{\boldsymbol{v}_i^{l+1}, \forall i \in N_v\right\}$. Specifically, we adjust the computation order of attention coefficients:

$$\alpha_{ij}^l = \frac{\exp\left((\boldsymbol{a}^l)^\top \text{LReLU}\left([\boldsymbol{v}_i^l \| \boldsymbol{e}_{ij}^l \| \boldsymbol{v}_j^l]\boldsymbol{d}_{ij}\right)\right)}{\sum_{k\in N_i} \exp\left((\boldsymbol{a}^l)^\top \text{LReLU}\left([\boldsymbol{v}_i^l \| \boldsymbol{e}_{ik}^l \| \boldsymbol{v}_k^l]\boldsymbol{d}_{ik}\right)\right)} \boldsymbol{dis}_{ij}, \tag{3}$$

where i is the target node and $j \in N_i$ is one of its neighbors, α_{ij}^l denotes the significance of node j relative to node i in layer l. This attention mechanism employs a learnable vector $\boldsymbol{a}^l$ to ensure consistent attention computation across nodes, while $\boldsymbol{d}_{ij}$ encodes edge directionality and $\boldsymbol{dis}_{ij}$ represents the distance-based attention weight. The concatenated features $[\boldsymbol{v}_i^l \| \boldsymbol{e}_{ij}^l \| \boldsymbol{v}_j^l]$ pass through the LeakyReLU activation function before the linear transformation, enabling the attention mechanism to adjust its weight allocation strategy dynamically. As a result, the model could more accurately characterize the interdependent relationship between EM and IR drop. Then the node representation is updated by aggregating attention coefficients and features from neighbors, followed by the activation function σ as:

$$\boldsymbol{v}_i^{l+1} = \sigma\left(\sum_{j\in N_i} \alpha_{ij}^l \boldsymbol{v}_j^l\right), \quad \forall i \in N_v. \tag{4}$$

In particular, the generated node embedding is used in the edge attention aggregator of the next layer, as shown in Figure 2. This crucial cross-task message passing allows the EM prediction path to incorporate local voltage and current context, thereby refining the stress prediction by accounting for localized Joule heating effects. However, increasing the model depth raises the risk of over-smoothing, a phenomenon where node representations become indistinguishable after multiple aggregations, leading to a loss of critical local features. Thus, we aggregate the node representations from all three NAA layers in our model, enabling the model to adaptively select the most appropriate neighborhood range information.

Edge Embedding Generation. Using the same input as the NAA layer, we leverage the graph attention network (GAT) -based edge attention aggregator (EAA) from [26] to collect information from neighboring nodes and edges, forming new edge features. For each edge, we treat its two end nodes and adjacent edges as its neighborhood node set. The input $\left\{\boldsymbol{v}_i^l, \forall i \in N_v\right\}$ and $\left\{\boldsymbol{e}_{ij}^l, \forall (i,j) \in N_e\right\}$ are integrated into a unified feature set $\left\{\boldsymbol{h}_k^l, \forall k \in N_c\right\}$, where N_c denotes the set of elements connected to the current edge. The output edge representations $\left\{\boldsymbol{e}_{ij}^{l+1}, \forall (i,j) \in N_e\right\}$ are generated as:

$$\boldsymbol{e}_{ij}^{l+1} = \text{EAA}\left(\boldsymbol{h}_q^l, \{\boldsymbol{h}_k^l \mid k \in N_c(q)\}\right), \text{where } q \to (i,j). \tag{5}$$

In addition, the generated edge embedding feeds into the next NAA layer, completing cross-task message passing. This enriches the IR drop path by leveraging EM's inherent high current dependency, enhancing hotspot detection accuracy. Like node embeddings, the edge representations from all three EAA layers are concatenated.

To enhance the physical consistency of EM-induced stress predictions and model interpretability, we integrate a PINN inspired by [11] within GEMIR. Taking edge feature embeddings $\{\boldsymbol{e}_{ij}^l, \forall (i,j) \in N_e\}$ as input, this PINN uses a 5-layer MLP with LeakyReLU activation to model nonlinear relationships between input features and stress evolution. Beyond data fitting, it explicitly encodes EM governing physics, such as atomic flux conservation and stress propagation described by Korhonen's PDE, ensuring stress representations align with both observed data and physical constraints to improve prediction reliability. The corresponding physical constraint loss is detailed in Section 3.4.

We obtain the final node and edge embedding after the attention aggregation introduced before, while the edge embedding and the PINN embedding are concatenated as the new final edge embedding with physics constraints. These are passed to the respective 2-layer MLP decoders for predictions.

3.4 Conflict-Gated Multi-task Optimization

Existing methods typically analyze EM and IR drop separately using single-task models. While effective for individual predictions, they neglect their interdependence and lack physical constraints, limiting their effectiveness on these related phenomena. To address this, we introduce new physics-informed constraints embedding physics laws such as the KCL equation and Korhonen's PDE with interpretability. However, simply combining these losses and gradients is not enough, as it faces the negative interference from work conflicts. To manage the complex optimization dynamics of joint learning, we propose a novel Conflict-Gated optimization strategy to deal with the conflict between the gradient from the IR drop and EM. This dynamic approach maximizes positive knowledge sharing while preventing negative interference, resulting in a robust optimization process that ensures mutual optimality and generalization. Notably, this strategy is only applied during training [21], introducing no additional inference cost.

3.4.1 *Loss Function Formulation.*

Data-driven Constraints. This component ensures the predictions align with the ground truth. The IR drop loss $\mathcal{L}_1$ and the EM-induced stress loss $\mathcal{L}_2$ are based on the mean squared error, respectively:

$$\mathcal{L}_1 = \frac{1}{|\mathcal{V}|}\sum_{v\in\mathcal{V}}\left(\hat{\boldsymbol{V}}_{ir,v} - \boldsymbol{V}_{ir,v}\right)^2, \mathcal{L}_2 = \frac{1}{|\mathcal{E}|}\sum_{e\in\mathcal{E}}\sum_{k=1}^{5}\left(\hat{\boldsymbol{\sigma}}_{em,e,k} - \boldsymbol{\sigma}_{em,e,k}\right)^2. \tag{6}$$

Physics-informed Constraints. To enhance the physical consistency and interpretability of the model, we introduce two physics-informed constraints. We integrate KCL constraints for IR drop prediction. According to KCL, the sum of the currents flowing in and out of the same node should be zero. As formulated in Equation (7), we define $\mathcal{L}_3$ as the sum of squared net currents at each node, where the current I_e of interconnect follows Ohm's law, calculated by the predicted values $\hat{V}_{ir,i}$ and $\hat{V}_{ir,j}$ at the two endpoints and the resistance R_e of this interconnect. $\mathcal{E}(v)$ denotes the set of edges incident to node v. We optimize this loss and hope it can

Table 2: Comparison with ML-based Multi-task Methods. The unit for MAE is $\times 10^{-4}V$, and for RMSE is $\times 10^{6}Pa$.

Methods	EGNN [6]			EDGe [4]			EMTM [26]			**GEMIR (Ours)**		
	MAE (IR drop) ↓	RMSE (EM) ↓	Runtime (Total) ↓	MAE (IR drop) ↓	RMSE (EM) ↓	Runtime (Total) ↓	MAE (IR drop) ↓	RMSE (EM) ↓	Runtime (Total) ↓	MAE (IR drop) ↓	RMSE (EM) ↓	Runtime (Total) ↓
Testcase7	1.61	–	2.05	1.37	3.54	**1.58**	0.78	2.52	2.97	**0.47**	**2.38**	2.74
Testcase8	1.75	–	1.74	1.44	3.26	**1.25**	0.94	3.30	2.66	**0.66**	**2.80**	2.53
Testcase9	2.31	–	2.87	2.88	6.97	**2.47**	1.49	**5.17**	3.36	**1.04**	7.02	3.23
Testcase10	2.75	–	2.26	2.47	5.22	**1.77**	1.28	**4.28**	2.37	**0.76**	6.05	2.26
Testcase13	5.53	–	1.38	4.76	9.12	1.72	2.25	7.63	1.33	**1.44**	**3.81**	**1.19**
Testcase14	2.13	–	1.32	2.85	6.91	1.98	3.61	12.19	1.58	**1.64**	**4.83**	**1.53**
Testcase15	2.43	–	1.96	1.86	4.63	**1.84**	1.08	3.65	2.29	**0.69**	**3.52**	2.12
Testcase16	2.91	–	2.02	9.32	22.27	**1.03**	2.05	6.93	2.37	**1.23**	**5.05**	2.03
Testcase19	3.68	–	2.73	3.75	6.74	**2.52**	1.27	**4.29**	2.96	**0.81**	4.63	3.01
Testcase20	0.96	–	2.88	3.97	2.41	3.29	0.64	2.16	3.28	**0.52**	**2.07**	**2.91**
Avg.	2.51	–	2.12	3.48	7.10	**1.95**	1.54	5.22	2.52	**0.92**	**4.21**	2.35

approach zero, penalizing any prediction that violates the KCL:

$$\mathcal{L}_3 = \sum_{v\in\mathcal{V}} \left(\sum_{e\in\mathcal{E}(v)} I_e \right)^2, \quad \boldsymbol{I_e} = \frac{\hat{\boldsymbol{V}}_{ir,i} - \hat{\boldsymbol{V}}_{ir,j}}{\boldsymbol{R_e}}. \tag{7}$$

For EM, we define $\mathcal{L}_4$ and integrate the constraints from the steady-state Korhonen's PDE, as formulated in Equation (8). This law governs the evolution of stress in interconnects. The static Korhonen's PDE is derived as a discrete second spatial derivative of stress in the steady state, which is also supposed to be 0. We calculate this derivative through a finite-difference approximation:

$$\begin{aligned} \mathcal{L}_4 &= \sum_{e\in\mathcal{E}} \left(\frac{\partial^2 \sigma_{em}}{\partial x^2} \Big|_{x_k} \right)^2, \\ \frac{\partial^2 \boldsymbol{\sigma}_{em}}{\partial x^2} &= \frac{\hat{\boldsymbol{\sigma}}_{em,e,k+1} - 2\,\hat{\boldsymbol{\sigma}}_{em,e,k} + \hat{\boldsymbol{\sigma}}_{em,e,k-1}}{(\Delta x_e)^2}, \end{aligned} \tag{8}$$

where $k \in \{1,2,3,4,5\}$ is the number of sampling points of the interconnect and Δx_e is the distance between adjacent sampling points on this interconnect. When boundary nodes are taken into account, the nearest nodes of adjacent edges are included in the calculation. This form ensures that the learned stress both fits the observed data and Korhonen's PDE in the steady state, especially for the enhancement from the PINN.

3.4.2 *The Conflict-Gated Strategy.*

A primary challenge in multi-task learning for EM and IR drop is managing the optimization dynamics. Although they are strongly related, their gradients on shared parameters are not always aligned. To exploit positive transfer while avoiding negative interference, we adopt an optimization strategy, CG. It fuses task gradients for synergistic knowledge sharing when they are aligned, and decouples updates for specialized learning when conflicts occur.

Stage1: Task-Level Gradient Unification. Let θ denote the parameters of GEMIR, and let θ_{ir} and θ_{em} be the parameters of the IR branch (node embedding generation and its decoder) and the EM branch (edge embedding generation and its decoder). The unified gradients for each task, $\boldsymbol{g}_{ir}$ (IR drop) and $\boldsymbol{g}_{em}$ (EM), are computed by summing their respective data-driven and physics-informed losses, as Equation (9) (where ∇ is the gradient operator). These gradients holistically represent the optimal descent direction for each task.

$$\boldsymbol{g}_{\text{ir}} = \nabla_\theta \left(\mathcal{L}_1 + \mathcal{L}_3\right), \ \boldsymbol{g}_{\text{em}} = \nabla_\theta \left(\mathcal{L}_2 + \mathcal{L}_4\right). \tag{9}$$

Stage2: Conflict-Gated Update Rule. We measure the alignment between task gradients using their inner product: $s = \langle \boldsymbol{g}_{\text{ir}}, \boldsymbol{g}_{\text{em}} \rangle$. A negative s indicates a conflict, while a non–negative s signals synergy. The CG selects branch updates as:

$$\boldsymbol{g}_{\text{node}} = \begin{cases} \boldsymbol{g}_{\text{ir}} + \boldsymbol{g}_{\text{em}}, & s \geq 0, \\ \boldsymbol{g}_{\text{ir}}, & s < 0, \end{cases} \boldsymbol{g}_{\text{edge}} = \begin{cases} \boldsymbol{g}_{\text{ir}} + \boldsymbol{g}_{\text{em}}, & s \geq 0, \\ \boldsymbol{g}_{\text{em}}, & s < 0. \end{cases} \tag{10}$$

The parameters are then updated with learning rate η. When $s \geq 0$, the fused gradient promotes robust shared representation learning. Conversely, decoupled updates prevent negative transfer. By dynamically switching between unified, synergistic updates and specialized, split updates, the CG maximizes beneficial knowledge transfer by leveraging the correlation and mutual influence of two tasks, while preserving task-specific accuracy.

4 Evaluation

4.1 Experimental Setup

Baselines. GEMIR is evaluated against three competitive ML-based methods. EGNN [6] enriches its node regression by aggregating both node and edge features and is widely used in node-level work. EMTM [26] jointly predicts thermomigration (TM) and EM-induced stress across multi-segment interconnects with accuracy and efficiency. EDGe [4] is a unified framework capable of predicting on-chip IR drop, EM, and temperature. However, it is not an end-to-end approach and must be retrained whenever the target changes.

Datasets. The ICCAD2023 [1] dataset is specialized in static IR drop prediction, featuring 20 real designs and 100 synthetic designs generated based on [5], closely resembling realistic PGs. This dataset is leveraged in Section 4.2 and Section 4.3. To assess the transferability and generalization of GEMIR, the public IBMPG [16] and Nangate [5] datasets are also employed in Section 4.4.

Metrics. To evaluate the performance of IR drop and stress prediction, the Mean Average Error (MAE) and Root Mean Square Error (RMSE) are respectively adopted as the metrics. The inference runtime is also considered to assess the efficiency of approaches.

Labels. EM-induced stress is computed based on the steady-state Korhonen's PDE under zero-flux boundary conditions using the numerical method in [18]. For IR drop, we employ the algebraic multigrid preconditioned conjugate gradient (AMG-PCG) method [16].

Table 3: Results of Evaluation for IR Drop.

Methods	MAE↓	F1↑	CC↑	MIRDE↓	Runtime↓
IRGNN [8]	0.83	0.72	0.97	2.89	6.22
LaRED [23]	1.02	0.70	0.94	2.77	1.76
GEMIR (Ours)	**0.77**	**0.75**	**0.98**	**2.44**	**2.35**

Table 4: Results of Evaluation for EM-induced Stress.

Methods	RMSE↓	MER↓	R^2 ↑	Runtime↓
EMGraph [12]	5.93	1.17%	0.76	1.44
HierPINN-EM [11]	6.56	1.22%	0.82	0.53
GEMIR (Ours)	**4.21**	**0.87%**	**0.89**	**2.35**

4.2 Performance of EM-IR Co-Analysis

Our GEMIR is first pretrained on fake designs from ICCAD2023 and then fine-tune on half of the real designs. The remaining ten real designs are used for testing. The accuracy and efficiency of our framework and other ML-based multi-task models are summarized in Table 2, which includes the metrics computed over all PG nodes. GEMIR consistently achieves the lowest IR drop MAE and EM-induced stress RMSE across all designs while maintaining efficiency. Compared with the state-of-the-art baseline EMTM, GEMIR achieves a significant average reduction of 40.79% in IR drop MAE and 19.35% in stress RMSE. The enhanced performance across both EM-induced stress and IR drop is attributed to modeling correlated physical fields with physics-informed constraints. Unlike models that may only loosely combine tasks, GEMIR's designed NAA and EAA with cross-task message-passing learn unified representations that are mutually enriched. In conclusion, GEMIR provides more reliable IR drop and EM predictions without significant runtime overhead compared with existing schemes.

4.3 Performance on Single Tasks

The GEMIR is assessed against single-task SOTA methods by evaluating jointly-trained models on individual targets Table 3 presents the prediction results for the IR drop. Compared to recent SOTA methods for IR drop prediction, the graph-based IRGNN [8] and the image-based LaRED [23], GEMIR achieves comparable or even superior performance in prediction at the bottom layer of the PG. On the metrics of MAE, F1 score, Pearson correlation coefficient (CC), and maximum IR drop error (MIRDE), our method has comparable and even better performance. The reduced MIRDE indicates that GEMIR is more accurate at severe IR drop hotspots. This suggests that using EM as a strongly related auxiliary task, together with KCL constraints, helps the shared representation better capture current-crowding regions that are difficult to learn from IR drop data alone. For EM prediction, results are presented in Table 4. GEMIR achieves a 29.01% reduction in RMSE and a 25.64% decrease in Mean Error Rate (MER), with better R-Square (R^2). The EM-focused PINN branch, regularized by the Korhonen-based physics loss, contributes significantly to this gain by enforcing physically consistent stress profiles along interconnect segments. Since the physics constraints are only used during training, these benefits come without extra inference cost. Also, this improvement is amplified by the auxiliary IR drop task. Overall, GEMIR matches or surpasses specialized single-task models on both IR drop and EM, while still supporting joint EM–IR analysis in a unified framework.

Table 5: Results of Transferring Study.

Methods	IBMPG [16]		Nangate [5]	
	MAE↓	RMSE↓	MAE↓	RMSE↓
EMTM [3]	0.68	2.74	0.47	3.32
GEMIR (Ours)	**0.33**	**2.25**	**0.24**	**2.51**

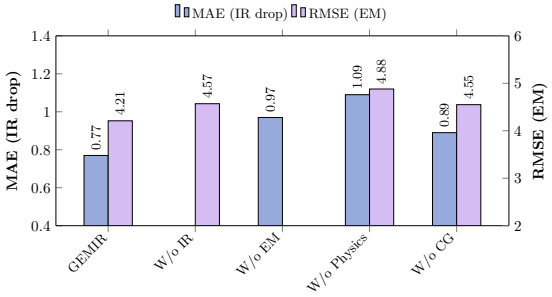

Figure 3: Results of Ablation Study.

4.4 Transferability on Unseen Designs

In practical sign-off flows, training data are often limited, and design styles can differ substantially across projects. To assess the transferability and generalizability of GEMIR, we utilize half data of IBMPG to fine-tune the pretrained model described in Section 4.2 and evaluate on the remaining IBMPG samples. The same procedure is applied to the Nangate dataset. Table 5 shows that GEMIR achieves strong generalization, providing better IR drop and EM-induced stress predictions compared to the previous method. Despite significant structural differences between different datasets, our framework shows robust performance. It demonstrates that GEMIR captures the underlying physical principles, not just dataset-specific correlations, making it highly suitable for practical application.

4.5 Ablation Study

Ablation studies are conducted to quantify the contribution of each key design in GEMIR. We compare the following schemes: (1) **W/o IR drop work** and (2) **W/o EM work**: the model is trained and evaluated only for the EM or IR drop task; (3) **W/o physics constraints**: removing both $\mathcal{L}_3$ and $\mathcal{L}_4$; (4) **W/o CG**: training GEMIR by combined loss without the CG optimization. As shown in Figure 3, disabling either the IR drop or EM branch harms the remaining task, verifying that EM supervision provides useful signals for IR drop and that IR drop distribution strongly drives EM-induced stress learning. These results collectively demonstrate the necessity of joint modeling, physics-informed constraints, and CG optimization.

5 Conclusion

The combined effects of EM and IR drop critically impact the reliability and power integrity of PGs. We propose a novel graph-based multi-task learning framework, GEMIR, designed to leverage the strong physical correlation between EM and IR drop and predict them simultaneously. Extensive experiments demonstrate that GEMIR successfully predicts both EM-induced stress and IR drop with superior performance and generalization.

References

[1] 2023. *CAD Contest at ICCAD.* https://www.iccad-contest.org/2023/Winners.html

[2] James R Black. 2005. Electromigration Failure Modes in Aluminum Metallization for Semiconductor Devices. *Proc. IEEE* 57, 9 (2005), 1587–1594.

[3] Vidya A Chhabria, Vipul Ahuja, Ashwath Prabhu, et al. 2021. Thermal and IR Drop Analysis Using Convolutional Encoder-Decoder Networks. In *IEEE/ACM Asia and South Pacific Design Automation Conference (ASPDAC)*. 690–696.

[4] Vidya A. Chhabria, Vipul Ahuja, Ashwath Prabhu, et al. 2023. Encoder-Decoder Networks for Analyzing Thermal and Power Delivery Networks. *ACM Transactions on Design Automation of Electronic Systems (TODAES)* 28, 1 (2023), 3:1–3:27.

[5] Vidya A Chhabria, Kishor Kunal, Masoud Zabihi, et al. 2021. BeGAN: Power Grid Benchmark Generation Using a Process-Portable GAN-Based Methodology. In *IEEE/ACM International Conference on Computer-Aided Design (ICCAD)*. 1–8.

[6] Liyu Gong and Qiang Cheng. 2019. Exploiting Edge Features for Graph Neural Networks. In *IEEE Conference on Computer Vision and Pattern Recognition (CVPR)*. 9211–9219.

[7] Feng Guo, Jiawei Liu, Jianwang Zhai, et al. 2024. PGAU: Static IR Drop Analysis for Power Grid Using Attention U-Net Architecture and Label Distribution Smoothing. In *ACM Great Lakes Symposium on VLSI (GLSVLSI)*. 452–458.

[8] Feng Guo, Yueyue Xi, Jianwang Zhai, et al. 2025. IRGNN: A Graph-based Framework Integrating Numerical Solution and Point Cloud for Static IR Drop Prediction. In *ACM/IEEE Design Automation Conference (DAC)*. 1–7.

[9] Feng Guo, Jianwang Zhai, Jingyu Jia, et al. 2025. IR-Fusion: A Fusion Framework for Static IR Drop Analysis Combining Numerical Solution and Machine Learning. In *IEEE/ACM Proceedings Design, Automation and Test in Europe (DATE)*. 1–7.

[10] Jingyu Jia, Jianwang Zhai, and Kang Zhao. 2024. Fast Estimation for Electromigration Nucleation Time Based on Random Activation Energy Model. In *IEEE/ACM Proceedings Design, Automation and Test in Europe (DATE)*. 1–2.

[11] Wentian Jin, Liang Chen, Subed Lamichhane, et al. 2022. HierPINN-EM: Fast Learning-Based Electromigration Analysis for Multi-Segment Interconnects Using Hierarchical Physics-informed Neural Network. In *IEEE/ACM International Conference on Computer-Aided Design (ICCAD)*. 1–9.

[12] Wentian Jin, Liang Chen, Sheriff Sadiqbatcha, et al. 2021. EMGraph: Fast Learning-Based Electromigration Analysis for Multi-Segment Interconnect Using Graph Convolution Networks. In *ACM/IEEE Design Automation Conference (DAC)*. 919–924.

[13] Wentian Jin, Sheriff Sadiqbatcha, Zeyu Sun, et al. 2020. EM-GAN: Data-Driven Fast Stress Analysis for Multi-Segment Interconnects. In *IEEE/ACM International Conference on Computer-Aided Design (ICCAD)*. 296–303.

[14] Matt A Korhonen, P Bo/Rgesen, King-Ning Tu, et al. 1993. Stress Evolution Due to Electromigration in Confined Metal Lines. *Journal of Applied Physics* 73, 8 (1993), 3790–3799.

[15] Subed Lamichhane, Mohamadamir Kavousi, and Sheldon X.-D. Tan. 2025. BPINN-EM: Fast Stochastic Analysis of Electromigration Damage using Bayesian Physics-Informed Neural Networks. In *IEEE/ACM International Conference on Computer-Aided Design (ICCAD)*. 1–9.

[16] Sani R Nassif. 2008. Power Grid Analysis Benchmarks. In *IEEE/ACM Asia and South Pacific Design Automation Conference (ASPDAC)*. 376–381.

[17] Jiwoo Pak, Bei Yu, and David Z Pan. 2015. Electromigration-aware redundant via insertion. 544–549.

[18] Zeyu Sun, Ertugrul Demircan, Mehul D. Shroff, et al. 2018. Fast Electromigration Immortality Analysis for Multisegment Copper Interconnect Wires. *IEEE Transactions on Computer-Aided Design of Integrated Circuits and Systems (TCAD)* 37, 12 (2018), 3137–3150.

[19] Matthias Thiele and Jens Lienig. 2018. *Fundamentals of Electromigration-Aware Integrated Circuit Design.* Springer.

[20] M Wang, Y Cheng, Y Lin, et al. 2024. MAUnet: Multiscale Attention U-Net for Effective IR Drop Prediction. In *ACM/IEEE Design Automation Conference (DAC)*. 1–6.

[21] Yuyang Ye, Mingwei He, Lizheng Ren, et al. 2025. Truly Pre-Routing Timing Prediction via Considering Power Delivery Network. In *ACM/IEEE Design Automation Conference (DAC)*. 1–7.

[22] Kin Fei Yong, Chin Theng Lim, and Wei Khoon Teng. 2022. System Level IR Drop Impact on Chip Power Performance Signoff for Risc-V System on Chip. In *IEEE/ACM International Microsystems, Packaging, Assembly and Circuits Technology Conference (IMPACT)*. 1–4.

[23] Chengxuan Yu, Yanshuang Teng, Wenhao Dai, et al. 2025. LaRED: Efficient IR Drop Predictor with Layout-Preserving Rebuilder-Encoder-Decoder Architecture. In *IEEE/ACM Proceedings Design, Automation and Test in Europe (DATE)*. 1–7.

[24] Xin Zhan, Peng Li, and Edgar Sánchez-Sinencio. 2016. Distributed On-Chip Regulation: Theoretical Stability Foundation, Over-Design Reduction and Performance Optimization. In *ACM/IEEE Design Automation Conference (DAC)*. 1–6.

[25] Yuxiang Zhao, Zhuomin Chai, Xun Jiang, et al. 2025. PDNNet: PDN-Aware GNN-CNN Heterogeneous Network for Dynamic IR Drop Prediction. *IEEE Transactions on Computer-Aided Design of Integrated Circuits and Systems (TCAD)* 44, 6 (2025), 2253–2263.

[26] Yunfan Zuo, Yuyang Ye, Hongchao Zhang, et al. 2024. A Graph-Learning-Driven Prediction Method for Combined Electromigration and Thermomigration Stress on Multi-Segment Interconnects. In *IEEE/ACM Proceedings Design, Automation and Test in Europe (DATE)*. 1–6.